SURFACE SCIENCE 28 (1971) 157–193 © North-Holland Publishing Co.

DESCRIPTION OF THE SiO_2–Si INTERFACE PROPERTIES BY MEANS OF VERY LOW FREQUENCY MOS CAPACITANCE MEASUREMENTS*

R. CASTAGNÉ and A. VAPAILLE

Institut d'Electronique Fondamentale, Bâtiment 220, Faculté des Sciences, 91–Orsay, France

Received 24 April 1971

Two measurement methods of the MOS capacitance under conditions of total reversibility are described. The knowledge of the exact very low frequency MOS capacitance permits us to determine for a given structure the apparent interface density in the whole band gap of silicon. We show theoretically that this apparent interface density can contain a contribution of defects unspecific of the interface, for instance: spatial fluctuation of the interface potential or silicon defects introducing a deep level in the band gap.
Experimental results show that: (1) the apparent interface density increases sharply towards the band edges; (2) in the structure having an important flat band translation the apparent interface state distribution can be attributed to the spatial fluctuation of the interface potential; (3) MOS structures having ⟨111⟩ orientation have an interface state distribution different from ⟨100⟩ homologous structures; for a ⟨111⟩ structure we find a peak of apparent interface density probably due to a donor defect in the silicon.

1. Introduction

Until recently, the most important results on the SiO_2–Si interface had been obtained from high or intermediate frequency MOS capacitance measurements. In this paper we want to show that the very low frequency (10^{-2} Hz) measurements can bring new interesting information about this interface.

The low frequency measurements are advantageous in the way they enable us to determine simultaneously:
– the surface potential value for a given bias,
– the complete interface state density in the whole band gap of the semiconductor using the same structure.

In section 2, we summarize the present knowledge on the SiO_2–Si interface and critically describe the classical methods of investigation. In section 3,

* This work is a part of a PhD thesis of R. Castagné, presented on 26 June 1970 at the Faculty of Sciences, Orsay, and registered under the number 680, serie A.

we point out that an apparent interface state density can be introduced by defects in the silicon or in the oxide. We are particularly concerned with deep defect levels in the silicon and with spatial fluctuations of the fixed oxide charge. In section 4, we describe our methods of investigation and we establish a criterion for the reversibility of the $C_{LF}(V)$ curves obtained experimentally*. In section 5, we finally describe our experimental results and give some interpretation of the most striking features of the $C(V)$ curves and of the density of state curves.

2. Summary of the known results on interface states and methods of investigation

Although their physical origin is not well established, the interface states are known to introduce energy levels in the band gap of the semiconductor and to be spatially localized in the interface. The electrical measurements, performed for instance on MOS capacitors or MOS FET, brought some information about:

(a) The repartition of the interface state density versus energy in some energy interval of the semiconductor band gap.

(b) The interface state capture cross-section.

(c) Their physical nature (donor states, acceptor states, ...) and origin.

The determination of the interface density of states $N_{ss}(\psi_s)$ ($cm^{-2}\ V^{-1}$) in the band gap, has been performed by many workers. This density seems to be at a minimum in the center of the gap. Gray and Brown[2]) found two peaks respectively near the conduction and the valence band edges. But according to Arnold[3]), Jund and Woehrn[4]), and Fahrner and Goetzberger[5]) (and also according to our own results), the density increases continuously towards band edges. We shall propose an interpretation of these observations in section 6.

It is well known that N_{ss} depends on the crystalline orientation of the surface, and that it is a minimum for the $\langle 100 \rangle$ and a maximum for the $\langle 111 \rangle$ silicon surface. Several workers[9]) have observed a correlation between the SiO_2 fixed charge density and the interface state density N_{ss}.

The interface state capture cross-sections have been measured extensively by Nicollian and Goetzberger[1]). Their results stand near $5 \times 10^{-15}\ cm^2$ in weak inversion and depletion regions. More recently, Fahrner and Goetzberger[5]) found that the cross-section decreases exponentially towards the band edges.

The interface state nature (donors or acceptors) is still a matter of dis-

* See the list of symbols at the end of this paper.

cussion. Some workers [2, 3] assume that they are acceptors in the higher half of the forbidden band and donors in the lower half; others argue on the opposite assumption. In fact, any measurement enables us only to determine a change in the interface charge after a variation of the surface Fermi level position; unfortunately, this variation is the same for acceptor and for donor centers.

Together with the interface states, some workers have also considered the possible existence of interface traps, spatially localized in the oxide, near the interface, and exchanging charges with the silicon by tunnel effect.

The most widely used tool to determine the surface state properties is the MOS capacitor. Its admittance is generally measured by adding a small ac signal to a fixed biasing potential. Depending on the ac signal frequency, three types of measurements can be made:

– In the very low frequency range ($f<0.1$ Hz) all the interface states and, eventually, the inversion layer follow the measurement signal without time lag. The $C_{LF}(V)$ curve obtained in this case will be referred to in what follows as a "reversible" curve.

– In the intermediate frequency range, dispersion phenomena occur due to the interface states or to the inversion layer. The high frequency limit of this range depends on the value of the interface state time constant and, then, on the value of the surface potential.

– In the high frequency range, the MOS structure is again a pure capacitance, $C_{HF\,limit}$, and is the result of series connection of the oxide capacitance, C_{ox}, and of the depletion layer capacitance, C_D. The various methods of determination of interface state density can be classified according to the frequency range in which the measurements are performed.

(a) *The low frequency methods.* From a low frequency curve $C_{LF}(V)$ one can determine, by means of the Berglund method [13]:

– the surface potential value $\psi_s(V)$ under an additive constant;

– the interface state capacitance $C_{ss}(\psi_s(V))$ by a comparison between the experimental value $C_{LF}(V)$ and the computed theoretical low frequency capacitance value.

The most important problem in working with Berglund's method is to be able to perform the C_{LF} measurement at a low enough frequency. If the ac signal frequency is too high, some interface states cannot contribute to the measured capacitance. In this case the determined variation of the surface potential is too large and the surface state density N_{ss} is incorrect. In section 5, we give an experimental criterion, leading to the choice of the measurement frequency. Although it is difficult to work correctly, Berglund's method proves to be a very powerful tool:

(1) the method is fast [especially by means of the ramp method [6, 14]];

(2) it gives the $\psi_s(V)$ value;

(3) it is the only one which allows us to determine, with a sufficient accuracy, the interface state density in the whole band gap of silicon, on the same structure.

(b) *The intermediate frequency methods.* Nicollian and Goetzberger[1]), and more recently, Fahrner and Goetzberger[5]), worked in the intermediate frequency range. From their measurements of the capacitance and of the equivalent parallel conductance, they brought a considerable amount of information on interface states and on the SiO_2–Si system in general. Though it is the most precise method, theirs is unfortunately quite slow and only gives information on a restricted part of the forbidden gap (between weak inversion and weak accumulation – this latter limit depending on the higher limit for the frequency of the ac signal).

(c) *The high frequency methods.* Terman's method[7]) uses the comparison between a high frequency measured $C_{HF}(V)$ curve and a computed theoretical high frequency curve. This method is easy and fast, but it only gives information on the same restricted part of the gap as does Nicollian and Goetzberger's method. Furthermore its precision is rather poor.

(d) *The static methods.* Somewhat different are the methods proposed by Gray and Brown[2]), Arnold[3]) and Jund and Woehrn[4]). These methods are often referred to as "static" methods. Gray and Brown measure the variation of the interface state charge after a displacement of the Fermi level in the bulk, due to a variation of temperature. The bias of the structure is adjusted to the flat band after each variation of the temperature.

Gray and Brown's method gives the surface state distribution in that part of the majority carrier half band swept by the Fermi level during cooling of the sample. The method proposed by Arnold, and by Jund and Woehrn, gives this density in a part of the minority carrier half band. The structure studied is a MOS FET and is biased at the inversion threshold during cooling.

3. Real and apparent interface state density

The interface states are due to defects spatially localized in the interface plane. In this section, we show that other defects, whose localization is not in the interface plane, can act on MOS capacitance curves in the same way as true interface states.

We are essentially concerned with two types of defect:

(1) deep level centers in the semiconductor;

(2) spatial fluctuations of the surface potential.

3.1. The effect of a semiconductor defect or impurity introducing a deep level in the semiconductor band gap on the MOS admittace

Defects or impurities which are present in the semiconductor substrate

and which introduce a deep level in the gap, will modify the $C(V)$ curves of a MOS structure[24]). They are responsible for two types of modification.

(a) They modify the space charge density and then the space charge width W at a given bias. Since this effect is responsible for a modification in the depletion layer capacitance of the structure, it can be revealed, in some cases by inspection of the $C_{HF}(V)$ curves.

(b) Because they can exchange charges with the conduction and valence bands of the semiconductor, they introduce either a dispersion phenomenon in the middle frequency range, or a mere additional capacitance, which looks like an interface state capacitance, in the very low frequency range.

3.1.1. *Space charge width modifications*

Let us consider for instance a p-type structure. We assume that the defect centers in silicon introduce a deep donor level in the lower half band gap. We suppose that this level stands at θ_R (in kT/q units) from the middle of the gap, and that $|\theta_R| < u_b$ (fig. 1).

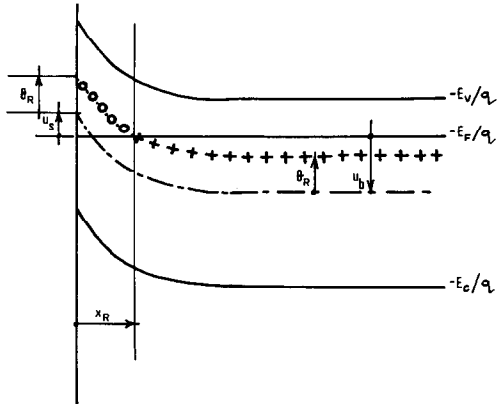

Fig. 1. Energy band near surface for a p-type structure with a deep level center.

(a) When the reduced surface potential u_s is larger than $-\theta_R$ the structure is in depletion, low inversion, the Fermi level goes through the deep level in a plane at a distance x_R from the interface (fig. 1). In the space included between the interface and this plane, the centers are neutral. The fixed ion density in space charge is nothing but the doping acceptor density N_A. Beyond this plane ($x_R < x$) the donor centers are positively charged. The fixed ion density in space charge is $N_A - N_R$.

(b) When $u_s < -\theta_R$, the structure is in depletion–accumulation. The Fermi

level does not intercept the deep level, so that the fixed ion density is $N_A - N_R$ in the whole space charge region.

We see from this discussion that when the Fermi level goes through the deep level, the space charge width W, and then the space charge capacitance C_D, vary more slowly with the surface potential than when there is no deep level. This ends in a break of the slope of the high frequency $C_{HF}(V)$ curve.

Furthermore, when the structure is biased in inversion, the high frequency capacitance is at a minimum $C_{HF\infty}$. The measured $C_{HF\infty}$ depends on the true space charge density in the depletion layer which is equal to N_A. On the other hand, if we measure the majority carrier concentration in the bulk, we find $p_{0b} = N_A - N_R$. The computed value of $C_{HF\infty}$, using this bulk doping concentration, is then smaller than the measured one.

In order to illustrate this discussion, we give in fig. 2, curves 1 and 2, the result of a theoretical computation of $C_{LF}(V)$ and $C_{HF}(V)$ curves for a p-type MOS structure with donor centers in a concentration of $N_R = 8.6 \times 10^{14}$ cm^{-3} in the silicon. These centers are assumed to introduce a deep level at $E_v + 0.35$ eV in the gap. The acceptor concentration is $N_A = 10^{15}$ cm^{-3}, so that the bulk majority carrier concentration is reduced to 2×10^{14} cm^{-3}. One can compare these curves with the curves 3 and 4 in the same figure, which give $C_{LF}(V)$ and $C_{HF}(V)$ for the same bulk concentration but without a deep level. One may notice the plateau in the $C_{LF}(V)$ (curve 1) and the difference in the minimum values in $C_{HF}(V)$ (curves 2 and 4).

3.1.2. *Modifications in the admittance of the MOS structure*

Charge exchanges between the deep level centers and the semiconductor valence and conduction bands, can be described by means of a distributed equivalent circuit[15, 6]). Fig. 3 represents the distributed circuit elements introduced by the centers standing between the planes x and $x + dx$. In this circuit the conductances G_{nR} and G_{pR} represent the charge exchanges between the deep level and the conduction and valence bands, respectively. C_R represents the charge accumulation on the centers:

$$G_{nR} = qc_n N_R [1 - f_{R0}(\theta_R, u(x))] \beta n_0(x) \, dx, \tag{1a}$$

$$G_{pR} = qc_p N_R f_{R0}(\theta_R, u(x)) \beta p_0(x) \, dx, \tag{1b}$$

$$C_R = qN_R f_{R0}(1 - f_{R0}) \beta \, dx. \tag{1c}$$

From these formulae, we see that the deep level capacitance $C_R(x)$ takes a significant value only in a small layer of width Δ, surrounding the plane of the abscissa x_R. In this volume, C_R takes the value

$$C_{RM}(\theta_R) = \tfrac{1}{4} q \beta N_R \Delta. \tag{2}$$

It can be shown[6]) that Δ is related to the space charge electrostatic field

$\mathscr{E}(\theta_R)$ in the plane x_R by

$$\Delta \simeq 6kT/q\mathscr{E}(\theta_R). \tag{3}$$

It should be noted that the field $\mathscr{E}(\theta_R)$ and the capacitance C_{RM} are not dependent on x_R.

For a very low frequency measurement, the dispersion phenomena do not have to be considered and the conductances disappear from the equivalent circuit.

This circuit is reduced to the capacitance C_{RM}, in plane x_R, which has to be incorporated in the low frequency equivalent circuit of the entire MOS structure. Fig. 4 gives, for example, the resulting equivalent circuit for a p-type structure in inversion with a deep level in the lower half of the forbidden gap. In this figure, C_{D1} represents the capacitance of the space charge layer extending between the surface and the plane x_R:

$$C_{D1} = \varepsilon_0 \varepsilon_{Si}/x_R; \tag{4}$$

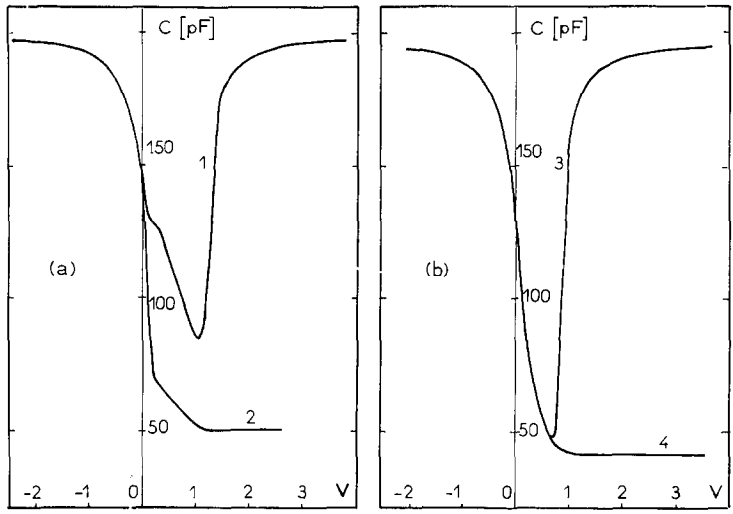

Fig. 2. Curves 1 and 2: Theoretical MOS curves with a deep level, p-type; $N_A = 10^{15}$ cm^{-3}, $N_R = 8.16 \times 10^{14}$ cm^{-3}, $E_R = E_v + 0.35$ eV, $p_{ob} = 2 \times 10^{14}$ cm^{-3}. Curves 3 and 4: Theoretical MOS curves without deep level; $N_A = p_{ob} = 2 \times 10^{14}$ cm^{-3}.

C_{D2} is the capacitance of the space charge layer going between x_R and the bulk

$$C_{D2} = \varepsilon_0 \varepsilon_{Si}/(W - x_R). \tag{5}$$

Though C_{RM} does not depend on x_R, its influence on the low frequency MOS capacitance C_{LF} depends on x_R, through C_{D1} and C_{D2} and, then, depends

on the surface potential ψ_s. The smaller x_R, the greater C_{D1}, and the greater the influence of C_{RM}.

Let us define the contribution C_{Req} of the deep level centers to the *apparent* interface state capacitance by

$$C_{R\,eq} = C_{RM} \frac{C_{D1}}{C_{D1} + C_{D2}}. \tag{6}$$

This contribution, depending on ψ_s through x_R, looks like a particular distribution of interface states.

Let us consider, for instance, the same p-type structures as in fig. 2, having a donor center introducing a level at $E_v + 0.35$ eV and a doping concentration such as $|u_b| > \theta_R$.

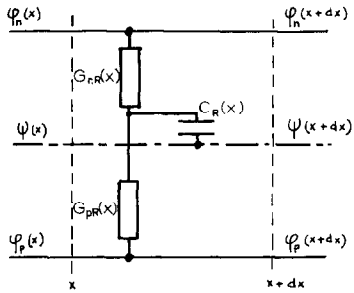

Fig. 3. Distributed circuit elements introduced by deep level centers standing between x and $x+dx$.

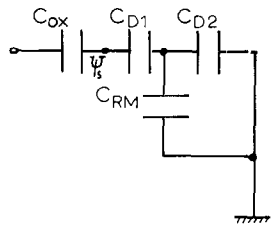

Fig. 4. Simplified equivalent circuits of MOS structure with a deep level; p-type, depletion.

(1) When $u_s < -\theta_R$, the Fermi level does not intercept the deep level and $C_{req} = 0$.
(2) When $u_s = -\theta_R$, the capacitance C_{Req} is maximum and equal to C_{RM}.
(3) When $u_s > -\theta_R$, C_{D1} becomes smaller and the capacitance C_{Req} becomes smaller too.

Then the localized deep level in the semiconductor looks like a peak in the interface state density and will be responsible for a plateau in the $C_{LF}(V)$ curve.

3.2. The effects of spatial fluctuations of the electrostatic potential in the SiO_2–Si interface plane

Nicollian and Goetzberger[1]) have considered the spatial fluctuations of the surface potential only for their effects on the parallel equivalent conductance of the structure. Estève[16]) introduces them in the analysis of the superficial leakage currents in planar junctions.

We have shown that these fluctuations can strongly modify the $C(V)$ curves of a MOS capacitor[17,18]), giving the appearance of an interface state density. It has been established[1]) that these fluctuations are essentially introduced by the inhomogeneities of the fixed positive charges in the oxide.

We shall consider the capacitance of the MOS structure, as the result of connecting in parallel, elementary capacitances of the same area α, in which the surface potential is uniform (fig. 5).

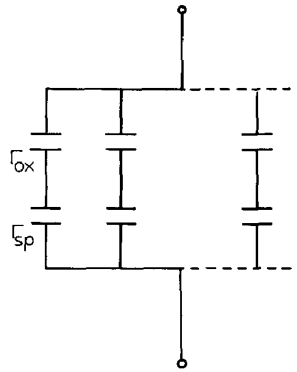

Fig. 5. The entire MOS capacitance results of parallel connection of elementary capacitances Γ_{ox} in series with Γ_{sp}.

Each of these capacitances is the result of connecting in series an elementary space charge capacitance Γ_{sp} whose value depends on the surface potential value (we assume this interface to be perfect, and then we ignore Γ_{ss}), and an elementary oxide capacitance Γ_{ox}.

We assume that the probability to find N positive charges in the oxide of one elementary capacitance is given by a Gaussian law

$$P(N) = \frac{1}{(2\pi\bar{N})^{\frac{1}{2}}} \exp\left(-\frac{(N-\bar{N})^2}{2\bar{N}}\right). \tag{7}$$

The positive charges in the oxide of an elementary capacitor obey a particular distribution law $n(x)$, x being their distance from the interface. We can define a mean distance X by

$$X = \frac{1}{\bar{N}} \int_0^{e_{ox}} x\, n(x)\, dx. \tag{8}$$

Then the total image charge *density* in the silicon of an elementary capacitor is

$$Q_i = -\frac{1}{\alpha} q \int_0^{e_{ox}} \frac{e_{ox}-x}{e_{ox}} n(x)\, dx = -\frac{q}{\alpha} N \frac{e_{ox}-X}{e_{ox}}. \tag{9}$$

The probability for an elementary capacitance to have an image charge density Q_i is then given by

$$P(Q_i)\,\mathrm{d}Q_i = P(N)\,\mathrm{d}N\,,$$

$$P(Q_i) = \frac{1}{[2\pi q\bar{Q}_i(e_{ox} - X)/\alpha e_{ox}]^{\frac{1}{2}}} \exp\left[-\frac{(Q_i - \bar{Q}_i)^2}{2q\bar{Q}_i(e_{ox} - X)/\alpha e_{ox}}\right]. \tag{10}$$

The standard deviation of this distribution is then

$$\sigma_{Q_i} = \left(q\bar{Q}_i \frac{e_{ox} - X}{\alpha e_{ox}}\right)^{\frac{1}{2}}.$$

When the entire MOS structure is biased under the potential difference of V, each elementary capacitance verifies that:

$$Q_i = (V - \psi_s + \psi_b)\,\Gamma_{ox} + Q_{Si}(\psi_s), \tag{11}$$

where $Q_{Si}(\psi_s)$ is the silicon charge which is reduced to the silicon space charge if the structure has no interface states.

Eq. (11) can be solved by iteration, in order to give, for each biasing potential value V, the surface potential ψ_s and the space charge capacitance $\Gamma_{sp}[\psi_s(V, Q_i)]$ corresponding to a given value of the image charge Q_i. Then the whole MOS capacitance can be computed from

$$C(V) = \int_{-\infty}^{\infty} \left(\frac{1}{\Gamma_{ox}} + \frac{1}{\Gamma_{sp}(V, Q_i)}\right)^{-1} P(Q_i)\,\mathrm{d}Q_i\,. \tag{12}$$

If the contribution of the minority carriers is taken into account in Γ_{sp}, eq. (12) gives us the low frequency MOS capacitance. In the other case, it gives the high frequency capacitance.

Theoretical values of the $C_{LF}(V)$ and $C_{HF}(V)$ curves were computed for an n-type structure with a doping concentration $N_D = 10^{15}$ cm^{-3}, an oxide capacitance $C_{ox} = 2 \times 10^{-8}$ F cm^{-2}, a standard deviation $\sigma_{Q_i} = 1.17 \times 10^{-8}$ C cm^{-2}, and a mean image charge $\bar{Q}_i = 8 \times 10^{-8}$ C cm^{-2} (corresponding to a flat band translation $\Delta V_{FB} = -4$ V). The results can be seen on fig. 6, curves 1 and 2.

It can be seen that the two $C(V)$ curves are spread along the bias axis, that $C_{LF}(V)$ becomes symmetrical around its minimum, and that this minimum is much higher than in the $C_{LF}(V)$ curves without fluctuation (see fig. 6, curves 3 and 4).

Curves having this appearance have frequently been observed for MOS structures with high image charge density. These curves have been interpreted generally by means of an interface state density.

If we consider the curves 1 and 2 of fig. 6 as experimental curves and simulate the determination of the apparent interface state density by various methods, we find the result shown in fig. 7. In this figure, curve 1 has been obtained by Berglund's method[13]), curve 2 by Terman's method[7]), curve 3 by Gray and Brown's method[2]), and curve 4 has been obtained by comparison between $C_{LF}(V)$ and $C_{HF}(V)$ (see section 5).

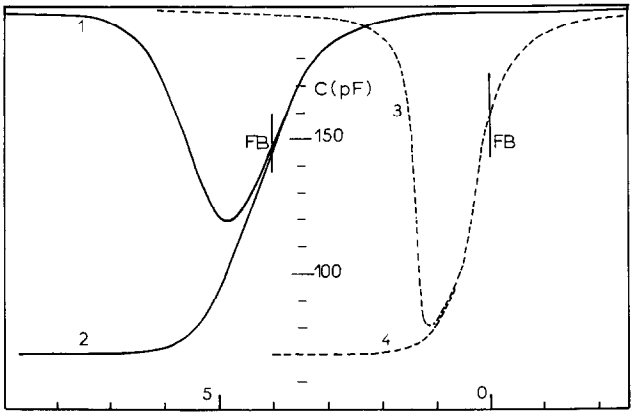

Fig. 6. Theoretical MOS curves showing the effect of the surface potential fluctuations. Curves 1 and 2: with fluctuations; curves 3 and 4: without fluctuations.

The apparent interface state density found, varies between 6×10^{10} and 6×10^{11} cm^{-2} V^{-1}. This apparent density should increase with the standard deviation σ_{Q_i}. This result could give an interpretation to the previously observed correlation between Q_f and N_{ss}. Arnold et al.[8]) find, for instance, for a mean density of image charge $\bar{Q}_i = 9 \times 10^{-8}$ C cm^{-2}, an interface state density of 4×10^{11} cm^{-2} V^{-1}.

The standard deviation σ_{Q_i} can also be written

$$\sigma_{Q_i} = (qQ_f)^{\frac{1}{2}}(e_{ox} - X)/\alpha e_{ox}, \tag{13}$$

which separates the effects of the mean oxide charge density Q_f from the effect of their mean distance X from the interface. This formula will be used throughout the discussion about our ion migration experiments which we shall report in section 5.

4. Proposed low frequency measurement methods and reversibility criteria

In order to obtain a true low frequency $C_{LF}(V)$ curve (hereafter referred to as a "reversible" curve), it is necessary that during the measurement, the

structure remain in a state very close to the thermodynamical equilibrium. Then the measured capacitance contains the total response of the interface states and eventually of the inversion layer.

In this section we shall describe the two frequency measurement methods which we proposed and used[14,19]), and we shall give the reversibility

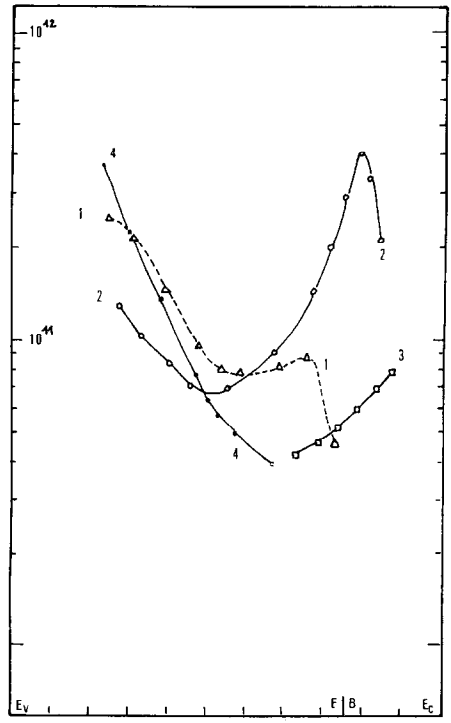

Fig. 7. Apparent interface state density introduced by surface potential fluctuations.

criterion for each of them. The first is the "ramp method". It has been used independently by Kuhn[20,21]) and by Kerr[22]). The second method[19]) is a very low frequency small signal method, hereafter referred to as the "rectangle method".

4.1. Ramp method

In the ramp method we measure[14]) the charging current of the MOS capacitor under a slow linear bias potential variation. This charging current is given by

$$i(t) = \frac{dQ}{dt} = \frac{dQ}{dV}\bigg|_{V(t)} \frac{dV}{dt} = a \frac{dQ}{dV}\bigg|_{V(t)} . \tag{14}$$

The quantity $(dQ/dV)|_{V(t)}$ is the differential capacitance of the structure for the instantaneous biasing potential $V(t)$. Plotting this current $i(t)$ versus $V(t)$, directly gives the $C_{LF}(V)$ curve. This curve is compared to the plot obtained with a standard capacitor under the same conditions. A block diagram of the apparatus is shown in fig. 8.

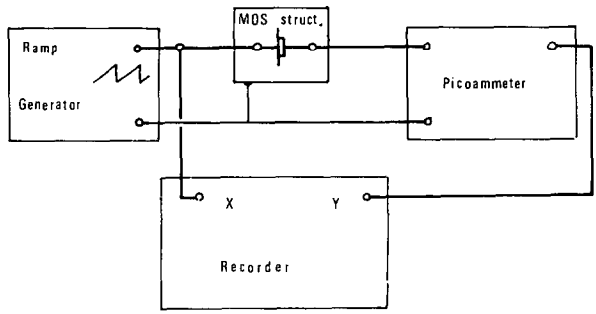

Fig. 8. Block diagram of the apparatus for ramp technique.

In addition to its great rapidity, this method takes advantage of the continuous plotting of the $C_{LF}(V)$ curve which clearly reveals the presence of a perturbation by surface states, deep level centers or hysteresis phenomena, etc. Its applicability is limited to the structures for which the leakage current remains small with respect to the charging current. Fig. 9 gives an example of the $C_{LF}(V)$ curve obtained by the ramp technique.

4.1.1. *Reversibility criterion for the ramp method*

When using the ramp method, and although the sweeping bias rate is a constant, the variation rate du_s/dt of the surface potential is not a constant: it is larger in the depletion and in the low inversion regions than in the accumulation or high inversion regions. Since the interface states and the inversion layer response depend on this surface potential variation rate, one must determine its value du_s/dt as a function of the surface potential u_s itself (for example, this has been done in fig. 10 for an n-type structure).

In order to establish the reversibility criterion for a $C_{LF}(V)$ curve obtained by the ramp method, one must verify whether the interface states, and eventually the inversion layer, can be equilibrated with the bulk for a given surface potential sweep rate.

(a) *Interface state response.* The charge in the interface state centers varies when the surface Fermi level sweeps their energy level. The centers whose energy level is in the upper half of the band gap exchange preferentially their

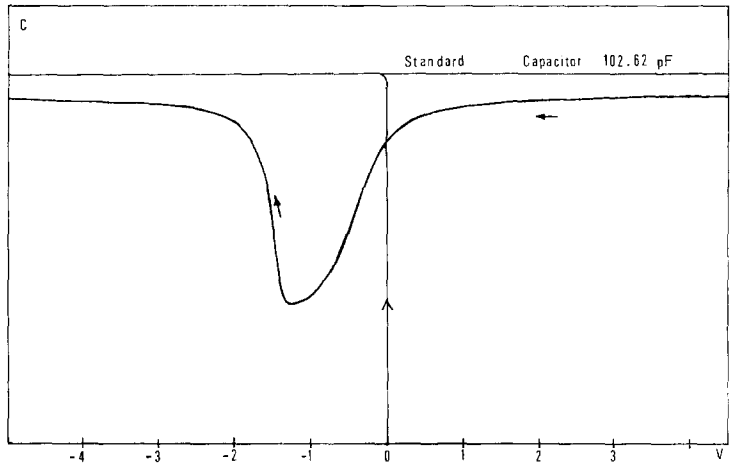

(a)

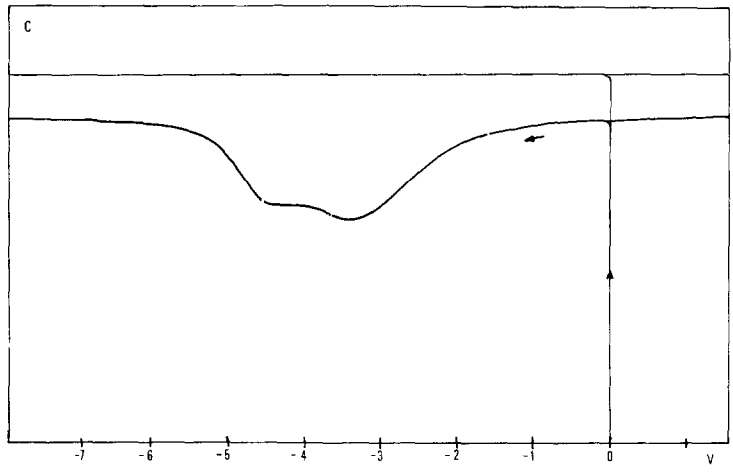

(b)

Fig. 9. An example of a C_{LF} curve obtained by the ramp technique. (a) n-type structure, 5 Ω, ⟨100⟩, $e_{ox} = 1400$ Å. (b) n-type structure, 1 Ω, ⟨111⟩, $dV/dt = 0.1$ V s^{-1}.

electrons with the conduction band. Their time constant is:

$$\tau_n(\theta) = (c_n n_i)^{-1} \exp(\theta). \tag{15}$$

The centers whose energy level is in the lower half of the band gap exchange their electrons with the valence band. Their time constant is

$$\tau_p(\theta) = (c_p n_i)^{-1} \exp(-\theta). \tag{16}$$

The occupation probability of a center whose energy level position is θ varies notably when the reduced surface potential u_s varies itself by ± 1 around the value $-\theta$. If this variation is performed in a time longer than the relaxation time τ_n or τ_p of the centers, these centers will reach equilibrium with the semiconductor bands without any noticeable delay.

The reversibility criterion for the interface states alone is then

$$\tau(\theta = -u_s)\frac{du_s}{dt} < 1. \tag{17}$$

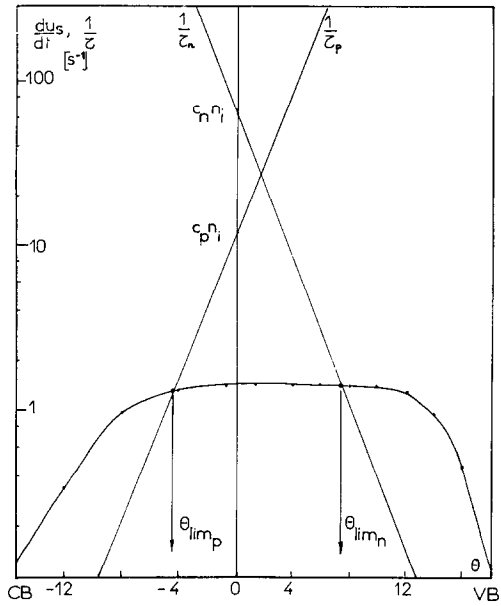

Fig. 10. du_s/dt, $\tau_n(\theta)^{-1}$, and $\tau_p(\theta)^{-1}$ versus $\theta = -u_s$.

(b) *The response of the whole structure.* Let us discuss, for instance, an n-type structure:

(1) When the Fermi level is in the upper half of the band gap, the reversibility criterion is reduced to that of the interface states and can be written

$$\tau_n(\theta = -u_s)\frac{du_s}{dt} < 1. \tag{18}$$

2) When the Fermi level is in the lower half of the band gap, the formation or the cancellation of the inversion layer is competing with capture or re-emission of the holes in the valence band, from the interface state.

The balance is then carried into effect through two steps:

– Equilibrium between the interface states and the valence band. It introduces a first reversibility criterion

$$\tau_p(\theta = -u_s)\frac{du_s}{dt} < 1 . \tag{19}$$

– Equilibrium between the inversion layer and interface states as a whole on one side, and the bulk on the other side. The recombination generation current in the space charge layer [which can be shown[23]) to be the most important source for minority carriers] must then fill or empty the inversion layer and the interface centers. When the condition (19) is verified, an equivalent circuit can be drawn as in fig. 11 for the structure in the inversion

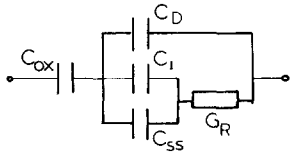

Fig. 11. Instantaneous equivalent circuit of a MOS structure in inversion.

region. Each element of this circuit must be evaluated for the instantaneous value of the biasing potential (instantaneous equivalent circuit): C_I and C_{ss} are the instantaneous values of the inversion capacitance and the interface states capacitance, respectively, and G_R is a conductance symbolizing the generation recombination phenomena in space charge.

From inspection of this instantaneous equivalent circuit one can see that the equilibrium of both inversion layer and interface states with the bulk introduces a second reversibility criterion, which is

$$\frac{C_{ss} + C_I}{G_R}\frac{du_s}{dt} < 1 . \tag{20}$$

4.1.2. *Testing the reversibility of a $C_{LF}(V)$ curve obtained by the ramp method*

Whichever the value of $u_s(t)$ may be, its sweep rate du_s/dt must verify (for an n-type structure), either the condition (18) when $u_s > 0$, or both conditions (19) and (20) when $u_s < 0$.

In order to test this, one can plot, as in fig. 10:

– the two straight lines giving respectively $*\tau_n(\theta)^{-1}$ and $\tau_p(\theta)^{-1}$;

– the curve giving du_s/dt versus u_s.

* Since the difficulties in the surface state equilibrium will be encountered only near midgap, one can take here for c_n and c_p the values given by Nicollian and Goetzberger[1]).

Let $\theta_{\lim n}$ and $\theta_{\lim p}$ be the values taken by u_s respectively when

$$\tau_n(u_s) = \left.\frac{du_s}{dt}\right|_{\theta_{\lim n}} \quad \text{and} \quad \tau_p(u_s) = \left.\frac{du_s}{dt}\right|_{\theta_{\lim p}}.$$

If we refer strictly to surface states equilibrium, the measured $C_{LF}(V)$ curve is a reversible one if $\theta_{\lim p}$ is closer to the conduction band than $\theta_{\lim n}$*. This means, in fact, that when the exchanges between the interface states and the conduction band are fading out, the exchanges with the valence band have already begun.

Finally, in order to test the last criterion, (20), it is necessary to measure the admittance of the MOS structure in the inversion region so as to determine the cut-off period $T(u_s)=(C_I+C_{ss})/G_R$.

With the n-type structure that we have chosen to illustrate this discussion, we found $T(u_s)=0.3$ s. One can see, in fig. 10, that the condition (20) is well verified.

4.2. THE "RECTANGLE" METHODS

To get reversibility of $C_{LF}(V)$ it is sometimes necessary (for instance, at a low temperature) to employ a very slow ramp ($dV/dt < 10^{-3}$ V s^{-1}). In that case the charging current is very small and the gain of the measuring system must be high. Furthermore, the measurement time has increased. The stability now becomes a problem.

In order to overcome these difficulties, we proposed to measure the $C_{LF}(V)$ capacitance by adding to the biasing potential, a small triangular ac signal. The amplitude of the triangular wave is fixed to kT/q (=25 mV at 20°C). The charging or discharging current is measured with the same system as in fig. 8. The plot $Y \propto i$ and $X \propto V$ on an X–Y recorder now has a rectangular shape. These plots are then compared to the plots given by a standard capacitor under the same conditions.

With this technique, it is quite easy to verify whether the measurement is made under the reversibility conditions. Fig. 12 represents the most general equivalent circuit for a MOS structure. The response of such a circuit to a triangular wave of amplitude A and frequency f is

$$i(t) = \pm 4AfC_{LF}[1 - \exp(-t/R_{Si}C_{LF})], \tag{21}$$

with

$$C_{LF} = C_{ox}C_{Si}/(C_{ox} + C_{Si}).$$

If the period $t=1/f$ of the triangular wave is much greater than the time

* A similar discussion can be found in ref. 25.

constant $R_{Si}C_{LF}$, the plot is a rectangle. If $t < R_{Si}C_{LF}$, the plot takes the shape of fig. 13.

Throughout this method, the reversibility criterion can be directly tested from mere inspection of the shape of the registered curves. It seems that it is most interesting to use a triangular wave instead of a sine wave.

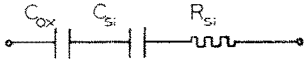

Fig. 12. Most general equivalent circuit for a MOS structure. C_{Si} = silicon capacitance (space charge and interface states), R_{Si} = silicon resistance which represents loss due to silicon space charge region or interface states.

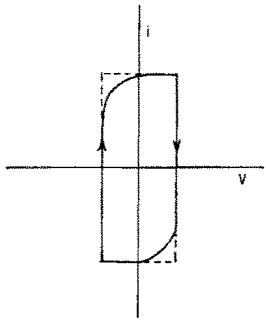

Fig. 13. An example of the plot obtained by the "rectangles" method when the reversibility conditions are not respected.

5. Experimental results and discussion

5.1. Experimental data process

In this section, we first describe how to deduce the surface potential and the surface state density N_{ss} from the experimental data. The experimental data consist of a $C_{LF}(V)$ curve obtained as it is described in section 4 and a high frequency $C_{HF}(V)$ curve measured with a Boonton 75 C bridge, generally at 500 kHz.

The process is as follows (the formulae are written for an n-type structure): (1) The surface doping concentration is computed from the high frequency capacitance in strong inversion using the formulae (see list of symbols at the end of this paper)[26]:

$$\frac{n_{0b}}{\log(n_{0b}/p_{0b})} = \left(\frac{C_{ox}C_{HF\infty}}{C_{ox} - C_{HF\infty}}\right)^2 \frac{2kT}{q^2\varepsilon_0\varepsilon_{ox}} \frac{1}{\mathscr{A}^2}. \tag{22}$$

(2) The flat band voltage is determined by: (a) computing the flat band capacitance

$$C_{FB} = \frac{C_{DFB}C_{ox}}{C_{ox} + C_{DFB}},$$

where[27])

$$C_{DFB} = \mathscr{A} q \left(\varepsilon_0 \varepsilon_{Si} \frac{n_{0b}}{kT} \right)^{\frac{1}{2}}; \tag{23}$$

and (b) reading on the $C_{HF}(V)$ curve the value V_{FB} of the bias potential corresponding to C_{FB}.

(3) The surface potential $\psi_s(V)$ is computed from the $C_{LF}(V)$ capacitance curve, through Berglund's formulae, by means of a computer

$$\psi_s(V) - \psi_b = \int_{V_{FB}}^{V} \left(1 - \frac{C_{LF}(V)}{C_{ox}} \right) dV, \tag{24}$$

ψ_b being the bulk potential deduced from the doping concentration.

(4) The density of interface states $N_{ss}(\psi_s)\ cm^{-2}\ V^{-1}$ is deduced from the surface state capacitance $C_{ss} = q\mathscr{A} N_{ss}$, which is computed through[19])

$$q\mathscr{A} N_{ss}(\psi_s) = C_{ss}(\psi_s(V)) = \frac{C_{ox} C_{LF}(\psi_s(V))}{C_{ox} - C_{LF}(\psi_s(V))} - C_D(\psi_s(V)), \tag{25}$$

where $C_D(\psi_s)$ is the computed value of the space charge capacitance.

(5) Another determination of the interface state density N'_{ss} can be made by comparing $C_{LF}(V)$ to the measured C_{HF} according to the formula[14])

$$q\mathscr{A} N'_{ss}(\psi_s) = \frac{C_{ox} C_{LF}}{C_{ox} - C_{LF}} - \frac{C_{ox} C_{HF}}{C_{ox} - C_{HF}}. \tag{26}$$

Such a determination is valid only in a limited interval of the forbidden gap. This interval extends from the inversion threshold to a value ψ_{s2} of the surface potential where the surface state time constant has become equal to the ac signal period. For instance, with a 500 kHz measurement frequency, the position ψ_{s2} is at about 250 mV from the majority carrier band edge. The higher the measurement frequency, the closer is ψ_{s2} to the majority carrier band edge[5]).

5.2. Experimental conditions

For the measurement, the MOS structures were placed in clean vacuum and in the dark. Furthermore, an ohmic contact was realized on the back of the structure and carefully verified. Such a precaution is highly important. If the back contact is not ohmic, it can be easily seen, as in fig. 14 (where C_c and G_c are the contact capacitance and conductance, respectively), that the high frequency measured capacitance is incorrect, being equal to $C_{MOS} C_c / (C_{MOS} + C_c)$. On the other hand, the low frequency measured capacitance is always true, being equal to C_{MOS}.

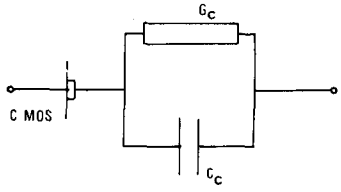

Fig. 14. Equivalent circuit for a MOS structure having a bad back contact.

5.3. Experimental results

The most important experimental results can be summarized as follows:
(1) The influence of the spatial fluctuations of the surface potential is very important on $C(V)$ curves, as well as on $N_{ss}(\psi_s)$ curves. In order to get confirmation of this influence, lithium ion migration in the oxide has been investigated.
(2) In every structure the interface state density continuously increases near both band edges. The observed states in these regions seem to have a very small capture cross section (i.e. they are slow states); this is true for $\langle 100 \rangle$ and $\langle 111 \rangle$ structures.
(3) The $\langle 111 \rangle$ structures present a peak in their apparent interface state density at about 0.35 eV from the valence band edge (this is true for p-type and n-type).

5.3.1. *An example of high quality structure*

A high quality n-type structure* (n-type, 5Ω, $\langle 100 \rangle$, $e_{ox} = 1400$ Å) has been measured. The experimental $C_{LF}(V)$ and $C_{HF}(V)$ curves are shown on fig. 15. One can see that they are very close to the corresponding theoretical curves which are shown on fig. 16.

No deformation of $C(V)$ curves is present; one can especially observe that the dissymmetry of the curves is conserved and that the flat-band translation is very small.

5.3.2. *General shape of $C_{LF}(V)$ and $N_{ss}(\psi_s)$ curves; influence of the spatial fluctuations of the surface potential*

We shall discuss as a characteristic example the curves obtained from two complementary units
p-type, 23 Ω, $\langle 100 \rangle$, $e_{ox} = 1400$ Å,
n-type, 5.5 Ω, $\langle 100 \rangle$, $e_{ox} = 1400$ Å,

* This structure has been provided by Sescosem Research Center Laboratory (91–Corbeville, France).

whose doping concentrations are equal and which contain an important interface state density.

Figs. 17 and 18 show their $C_{LF}(V)$ and $C_{HF}(V)$ (500 kHz) curves. We can remark that the $C_{LF}(V)$ curves turn to be symmetrical around their minimum value and to spread along the bias axis.

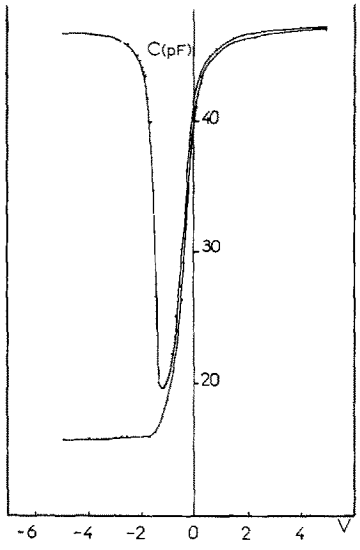

Fig. 15. An example of good structure; n-type, 5 Ω, ⟨100⟩. Dry oxide, $e_{ox} = 1400$ Å.

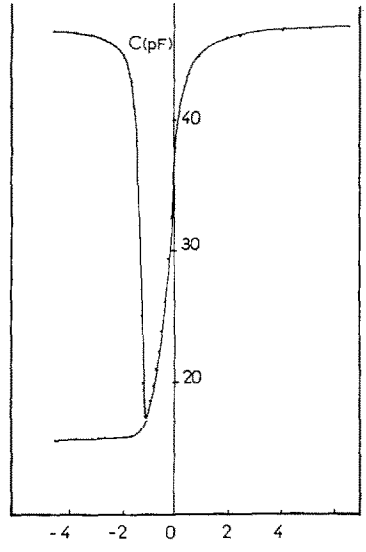

Fig. 16. Theoretical curves for the structure of fig. 15.

It is possible to interpret these curves in a classical way, using an interface state distribution. This has been done on the curves of figs. 19 and 20, giving $N_{ss}(\psi_s)$ and $N'_{ss}(\psi_s)$ interface state densities.

We first remark that the $N_{ss}(\psi_s)$ curves for n-type and p-type have a similar shape under a symmetry around the middle of the gap. Such a feature would indicate that the interface state density is dependent on the type of doping, according to the same law for p-type and for n-type. This is not likely to occur.

We also remark, for the two structures, a peak in the $N_{ss}(\psi_s)$ curve, always near the flat band region. When the bulk Fermi level position is changed (by modifying the temperature of the sample), the peak in $N_{ss}(\psi_s)$ follows the flat band position.

We have shown in section 3 (figs. 6 and 7) the modifications introduced by the fluctuations of the surface potential on the $C_{LF}(V)$, $C_{HF}(V)$, and $N_{ss}(\psi_s)$ curves. A comparison between the experimental curves of figs. 17–20 for p-

and n-type structures, and the curves of figs. 6 and 7 shows that the first ones can be interpreted by the effects of spatial fluctuations of the surface potential. Furthermore, we have computed the $N_{ss}(\psi_s)$ density, using for $C_D(\psi_s)$ a theoretical value and taking into account the fluctuations [the standard deviation being chosen by comparison between the experimental and theore-

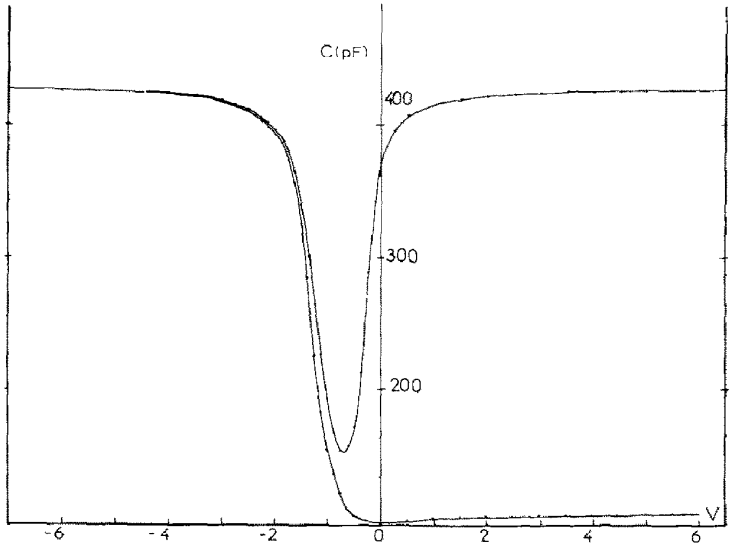

Fig. 17. Experimental $C_{LF}(V)$ and $c_{HF}(V)$ curves for p-type structure; 23 Ω, ⟨100⟩, $e_{ox} = 1400$ Å.

tical corresponding $C_{LF}(V)$ curve]. We have obtained for the previous p- and n-type structures, the curves in figs. 21 and 22. We observe that the peaks at the flat band disappear and that the density of the interface states becomes symmetrical around the mid-gap.

In order to confirm this interpretation, we have worked on ion migration in the oxide. These experiments will now be reported.

5.3.3. *Confirmation of the influence of the potential fluctuations: lithium ion migration experiments*

Lithium was introduced in the oxide of various structures, using an implantation technique through the aluminium gate. This procedure is advantageous because it introduces only one type of ion in a restricted quantity.

During the migration experiments, the structure was heated to about 80 °C and then positively or negatively biased for a given time. The measure-

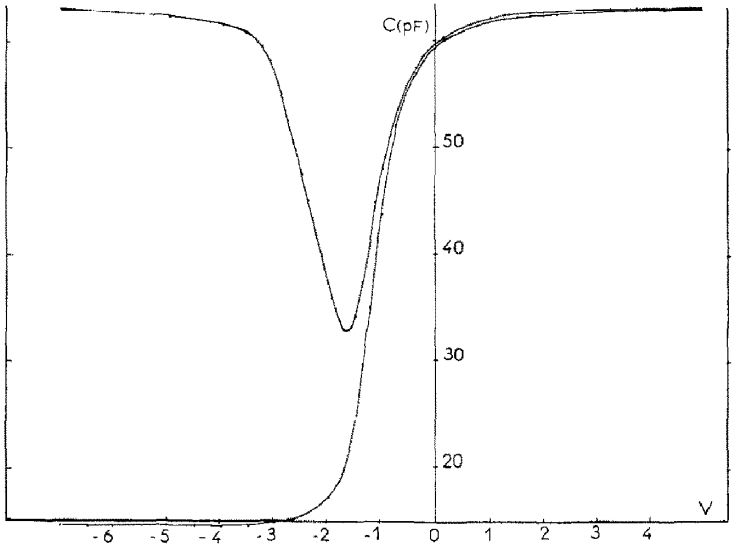

Fig. 18. Experimental $C_{LF}(V)$ and $C_{HF}(V)$ curves for n-type structure; 5.5 Ω, ⟨100⟩, $e_{ox} = 1400$ Å.

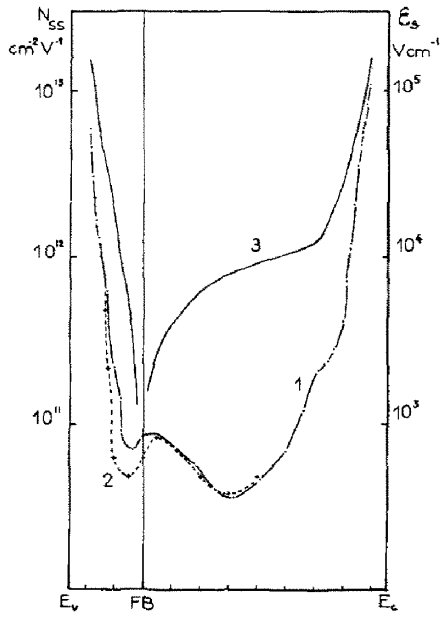

Fig. 19. $N_{ss}(\psi_s)$ and $N'_{ss}(\psi_s)$ interface state densities for p-type structure of fig. 17. Curve 1: $N_{ss}(\psi_s)$, curve 2: $N'_{ss}(\psi_s)$; curve 3: $\mathscr{E}_s$.

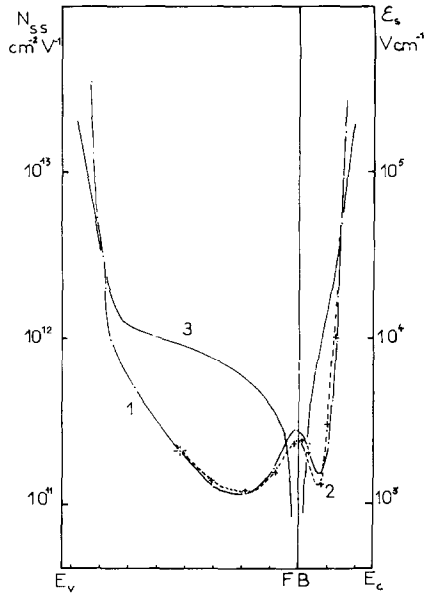

Fig. 20. $N_{ss}(\psi_s)$ and $N'_{ss}(\psi_s)$ interface state densities for n-type structure of fig. 18. Curve 1: $N_{ss}(\psi_s)$, curve 2: $N'_{ss}(\psi_s)$; curve 3: $\mathscr{E}_s$.

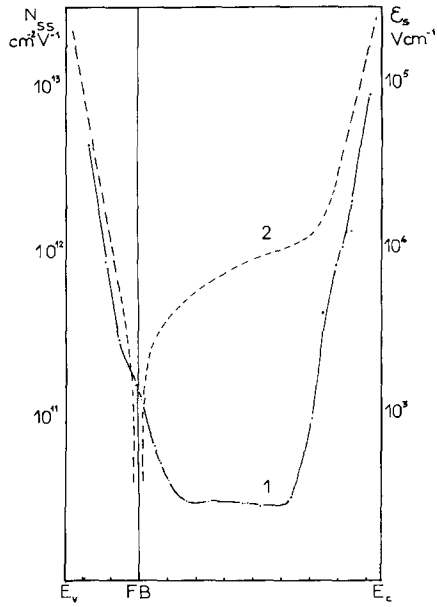

Fig. 21. $N_{ss}(\psi_s)$ obtained from experimental data of fig. 17 (p-type structure) and a theoretical curve taking into account the surface potential fluctuations.

ments were performed after cooling down to −30°C. At this temperature, the Li ions are fixed.

A typical result, obtained with an n-type structure, ⟨100⟩, 5 Ω, $e_{ox} = 1400$ Å, is shown on fig. 23, giving $C_{LF}(V)$ and $C_{HF}(V)$ after various migrations. Curves 0 – before ion implantation; curves 1 – after ion implantation; curves 2 – after a first migration (−15 V, 90°C, 1 hr); curves 3 – after a second migration (+6 V, 60°C, 1 hr); curves 4 – after a third migration (−10.5 V, 70°C, 1 hr).

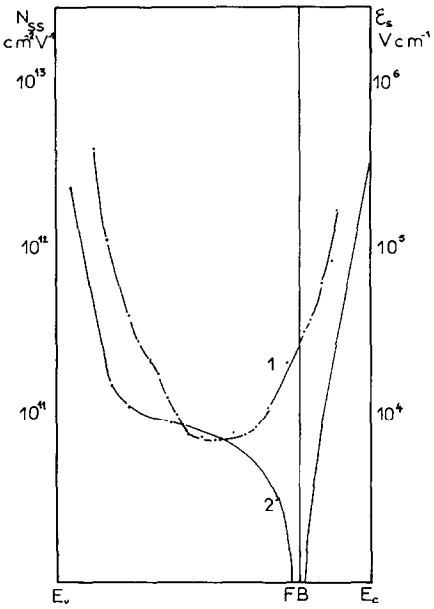

Fig. 22. $N_{ss}(\psi_s)$ obtained from experimental data of fig. 18 (n-type structure) and a theoretical curve taking into account the surface potential fluctuations.

After a migration under positive bias, the positive Li ions are moving towards the interface. One can see that the flat band translation increases and that the curves spread along the bias axis. The $C_{LF}(V)$ curves also, get more and more symmetrical, and their minimum value increases. After a migration under negative bias, we observe strictly opposite effects.

After each migration, the $N_{ss}(\psi_s)$ curve was computed. Fig. 24 shows these different curves. It should be noted that the shape of these curves is very close to the theoretical curve 1 of fig. 7. It can also be seen that the apparent density of interface states increases with flat band translation, i.e., with image charge.

Another observation is that the parallel conductance curves $G(V)$ are not

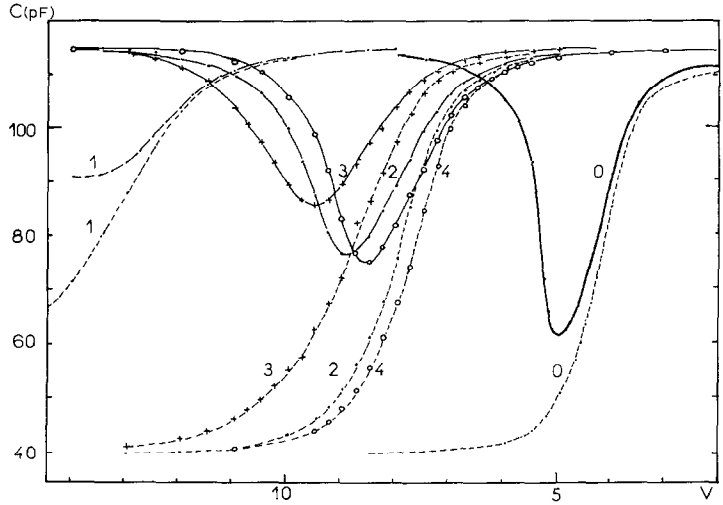

Fig. 23. Experimental $C_{LF}(V)$ and $C_{HF}(V)$ curves for n-type structure, 5 Ω, ⟨100⟩, $e_{ox} = 1400$ Å, after various migrations of Li implanted ions. Curves 0: before ion implantation; curves 1: after ion implantation; curves 2: after first migration, −15 V, 90 °C, 1 h; curves 3: after second migration, +6 V, 60 °C, 1 h; curves 4: after third migration, −10.5 V, 70 °C, 1 h.

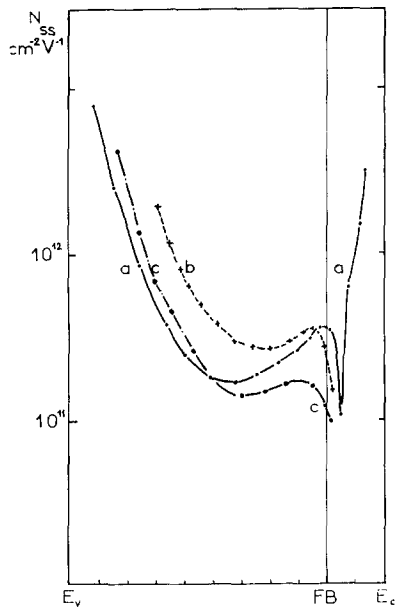

Fig. 24. $N_{ss}(\psi_s)$ curves computed after each ion migration. (a) after first migration; (b) after second migration; (c) after third migration.

appreciably modified by the various migrations (fig. 25). This indicates that the losses on interface states and, consequently, the number of actual interface states, are not significantly modified by the migrations.

During any migration, the total charge of positive ions in the oxide does not vary. Only the image charge $\bar{Q}_i$ is changed because of the mean position X of the positive ions. At the same time, the standard deviation σ_{Q_i} has varied, as it can be seen in eq. (13).

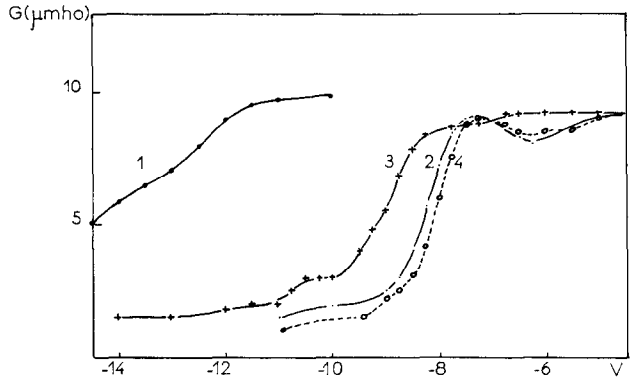

Fig. 25. Experimental G(V) curves after each migration.

These two remarks explain, by the fluctuations, the observed evolution of the $C(V)$ curves. They also explain the shape and the evolution of the $N_{ss}(\psi_s)$ curves.

If this evolution was due to real interface states, these defects might be apt to appear or to disappear reversibly under the migration treatment. The defect model proposed by Goetzberger, Heine and Nicollian[10]) might explain this behavior, but such defects would induce simultaneous modification of the $G(V)$ curves, which was not observed.

Finally, we tried to determine the standard deviation fitting the best with the experimental $C_{LF}(V)$ and $C_{HF}(V)$ curves. Fig. 26 gives an example (for third migration). For the experimental curves of fig. 23, the best fit was obtained with the following values of σ_{Q_i}:

Curve 1, $V_{FB} = -12.5$ V, $\sigma_{Q_i} = 2 \times 10^4$ pC cm^{-2},
Curve 2, $V_{FB} = -7.4$ V, $\sigma_{Q_i} = 1.6 \times 10^4$ pC cm^{-2},
Curve 3, $V_{FB} = -8.1$ V, $\sigma_{Q_i} = 1.7 \times 10^4$ pC cm^{-2},
Curve 4, $V_{FB} = -7.1$ V, $\sigma_{Q_i} = 1.48 \times 10^4$ pC cm^{-2}.

For the successive migrations, $\sigma^2_{Q_i}$ seems to vary linearly with V_{FB}. We also see on fig. 26 that, to obtain a better fit it would be necessary to consider σ as a function of the surface potential (we think of another type of fluctuation)

taking higher values in the depletion than in the accumulation region. This result is in agreement with the recent publication by Fahrner and Goetzberger[5]).

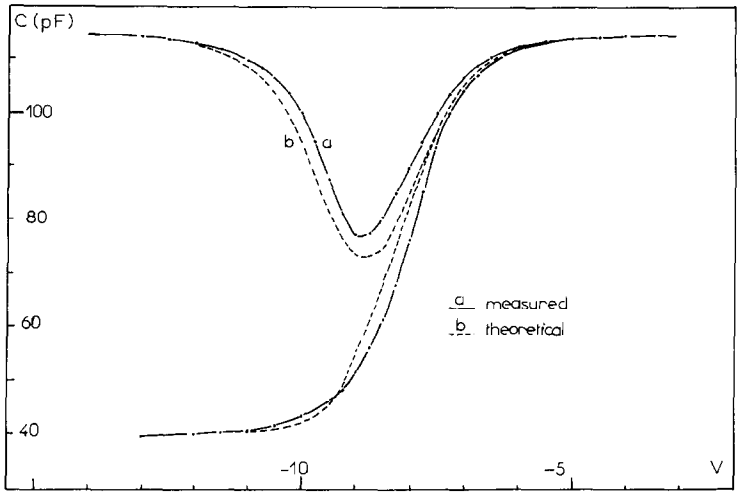

Fig. 26. An example of a fit between the experimental curves 4 of fig. 23, and theoretical curves with fluctuations ($\sigma_{Q_1} = 1.48 \times 10^4$ pC cm^{-2}).

5.3.4. *General shape of the $N'_{ss}(\psi_s)$ curves*

The $N'_{ss}(\psi_s)$ curves were computed from experimental $C_{LF}(V)$ curves and $C_{HF}(V)$ curves measured at 500 kHz. Figs. 19 and 20, curves 2, give an example. Two important features may be noticed:

(1) *The $N'_{ss}(\psi_s)$ density of states shows a hook in the weak accumulation region.* When the structure is biased in weak accumulation, the interface states become able to follow the high frequency measurement signal. They can no longer contribute to $N'_{ss}(\psi_s)$ which decreases. To support this explanation, we can for instance perform the $C_{HF}(V)$ measurement at a lower frequency. Fig. 27 shows $N'_{ss}(\psi_s)$ for a 5 kHz measurement. We see that the cut-off region has shifted away from the majority carrier band edge.

From the $C_{LF}(V)$ and $C_{HF}(V)$ capacitance measured, with a biasing potential corresponding to the cut-off, one can compute the time constant τ of the interface states and, then, their capture cross-section. This has been done for instance for a p-type structure at two temperatures:

for $T = -31\,^\circ$C, we find $\sigma_p = 5.2 \times 10^{-16}$ cm^{-2},

for $T = 80\,^\circ$C, we find $\sigma_p = 2.6 \times 10^{-16}$ cm^{-2}.

The capture cross-section of the centers is decreasing when the temperature increases, which would indicate that they are attracting centers.

(2) *The $N'_{ss}(\psi_s)$ density of states rises sharply towards majority carrier band edge in the strong accumulation region.* This feature can be noticed also on the $N_{ss}(\psi_s)$ curves for both band edges, and will now be discussed.

5.3.5. *Increase of $N_{ss}(\psi_{ss})$ and $N'_{ss}(\psi_{ss})$ densities near band edges*

We always observed that the $N_{ss}(\psi_{ss})$ and $N'_{ss}(\psi_{ss})$ densities sharply increased towards band edges in strong accumulation. We have good reasons to believe that these interface states, located near the band edges, are slow states. For instance, they are also seen on the $N'_{ss}(\psi_s)$ curve of fig. 27, which is determined from a 5 kHz C_{HF} measurement. This shows that even in this part of the gap, these states do not respond to such a low frequency*.

On the other hand, the observed phenomenon is reversible under surface potential variations: $C_{LF}(V)$ curves do not show any hysteresis in their accumulation or inversion region. We must then exclude any interpretation based upon charge injection in the oxide.

The increase towards band edges looks exponential in ψ_s. Two parameters are exponentially increasing as the Fermi level moves towards the band edges: the surface carrier concentrations n_s or p_s, and the electric field $\mathscr{E}_s$ at the interface.

To account for the high relaxation time of these states, it seems necessary to introduce a trapping phenomenon following the model of Heiman and

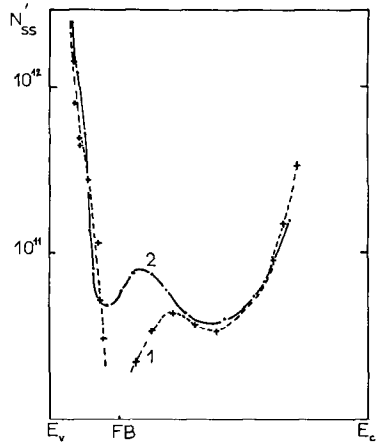

Fig. 27. $N'_{ss}(\psi_s)$ curve from a 5 kHz $C_{HF}(V)$ measurement (curve 1), and a 500 kHz $C_{HF}(V)$ measurement (curve 2) for a p-type structure as in fig. 17.

* Fahrner and Goetzberger[5]) have also observed an increase in the interface state density and an exponentially decreasing surface state capture cross-section towards the band edges.

Warfield[11]). The trap centers should also be spatially distributed in the oxide, away from the interface.

In order to explain the exponential increase of the measured interface state density towards the band edges, one must assume:
– either an exponential increase of the density $N_t(x)$ of the trap centers with the distance x, in the oxide, from the interface[28]),
– or a displacement of the trap centers under the high electrical field at the interface when the structure is in strong accumulation or in strong inversion.

We reported in figs. 19–22 the surface electric field variations versus ψ_s. We see that $N_{ss}(\psi_s)$ and $N'_{ss}(\psi_s)$ density variations are very similar to the $\mathscr{E}_s$ variations.

For this reason, we have sought a link between the fast increase of the interface state density near the band edges, and the similar increase of the surface field $\mathscr{E}_s$. Let us assume:
(1) That there is, between SiO_2 and Si, a nonstoichiometric layer whose properties can vary when the electric field at the interface is high.
(2) That this layer contains an equal number of positively and negatively charged centers. According to Goetzberger, Heine and Nicollian[10]), such centers can, under a certain condition, induce "classical" interface states in the center of the silicon band gap*. But we furthermore assume that they can capture, by tunnel effect, either electrons (the positive centers) or holes (the negative centers).
(3) To explain the increase of interface state density near band edges, we finally assume that the centers can displace themselves under the strong interfacial electrostatic field.

When $\mathscr{E}_s$ is directed towards the interface (n-type/structure in accumulation, p-type structure in inversion), the positive centers are shifted towards the interface. Because their capture cross-section is exponentially increasing, there are more centers able to capture electrons. When $\mathscr{E}_s$ is directed towards the SiO_2 (n-type structure in inversion, p-type structure in accumulation) the negative centers are now attracted and they capture the holes.

Such a mechanism can explain the results obtained by Arnold[3]), and by Jund and Woehrn[4]), because, in their experiments, the lower the temperature, the greater was the electric field at the inversion threshold. On the other hand, Gray and Brown[2]), doing their measurements in the flat band position ($\mathscr{E}_s = 0$), could not see any increase of the number of trapping sites, nor any increase of the interface state density near band edges. This is in agreement with their results.

* It is noticeable that for the various structures we have studied, the interface state density near mid-gap and near band edges varied in the same way and in an almost equal proportion, after each treatment or from one structure to another.

5.3.6. *Peculiarities of the* SiO_2–Si *interface with* $\langle 111 \rangle$ *crystal orientation*

Many MOS capacities grown on silicon crystal with surface crystallographic orientation $\langle 111 \rangle$ were investigated with the previously described methods. The low frequency curves $C_{LF}(V)$ and the high frequency curves $C_{HF}(V)$ always appeared very different from the curves obtained with $\langle 100 \rangle$ identical structures.

For example, we give in fig. 28 the curves obtained from three $\langle 111 \rangle$ structures:
fig. 28a, n-type, $\langle 111 \rangle$, 5.8 Ω, $e_{ox} = 1400$ Å;
fig. 28b, n-type, $\langle 111 \rangle$, 1.1 Ω, $e_{ox} = 1400$ Å;
fig. 28c, p-type, $\langle 111 \rangle$, 27 Ω, $e_{ox} = 1400$ Å;
and we also give in fig. 28d, for comparison, the curves $C_{LF}(V)$ and $C_{HF}(V)$ of an n-type $\langle 100 \rangle$ structure (5.5 Ω, $e_{ox} = 1400$ Å). This last structure and the first n-type $\langle 111 \rangle$ structure in fig. 28a have been fabricated together.

We see that the curves $C_{LF}(V)$ from $\langle 111 \rangle$ structures show a "plateau" in the low inversion region of the n-type structures or in the low depletion region of the p-type structures. The slope of the $C_{HF}(V)$ curves shows a break in the same regions. These features are never observed in the curves of the $\langle 100 \rangle$ structures.

For the n-type $\langle 111 \rangle$ MOS capacitances, we also remarked that the doping concentration N_D computed from $C_{HF\infty}$ was always greater than the doping concentration measured in the bulk. For instance, for the structure in fig. 28a, we found from C_{HF}: $N_D = 1.5 \times 10^{15}$ cm^{-3}, and from the bulk resistivity: $N_D = 9 \times 10^{14}$ cm^{-3} (this is not valid for p-type $\langle 111 \rangle$ structures).

If we compare all these observations to the theoretical previsions of section 2.1 for a MOS structure with a deep defect in silicon, we see that they are in accord on most of their aspects: the plateau in $C_{LF}(V)$ is observed on both experimental and theoretical curves. The break in the $C_{HF}(V)$ curves and the increase of their minimum values $C_{HF\infty}$ are also observed in both experimental and theoretical curves.

We shall try to explain the peculiarities observed on the experimental curves for $\langle 111 \rangle$ structures by the existence of a defect in a small layer of the silicon, near the interface.

Our experimental results bring confirmation of three points:
(1) The observed defect introduces a localized defect level in the band gap. Using the notations of section 2.1, we note that the capacitance contribution of the centers is maximum when $x_R = 0$. Then the "plateau" appears in the $C_{LF}(V)$ curves when the Fermi level intercepts the deep level just on the interface plane. We show in figs. 28a–c the surface potential $\psi_s(V)$ variations versus the bias. It can be seen that the middle of the plateau of the $C_{LF}(V)$

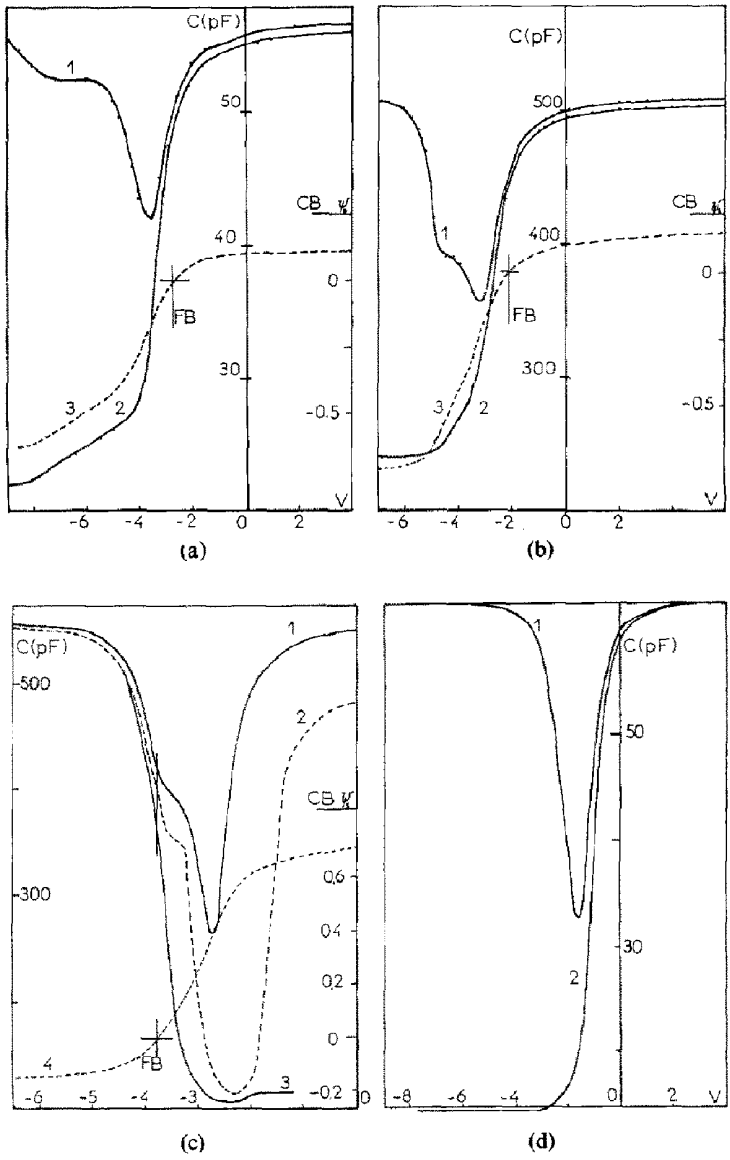

Fig. 28. Experimental $C_{LF}(V)$ and $C_{HF}(V)$ curves for various ⟨111⟩ MOS structures. (a) n-type, 5.8 Ω, ⟨111⟩, $e_{ox} = 1400$ Å; (b) n-type, 1.1 Ω, ⟨111⟩, $e_{ox} = 1400$ Å; (c) p-type, 27 Ω, ⟨111⟩, $e_{ox} = 1400$ Å; and for comparison with (a), (d) n-type, 5.5 Ω, ⟨100⟩, $e_{ox} = 1400$ Å, elaborated together with the structure of (a).

curves corresponds to the position $E_v + 0.35$ eV of the surface Fermi level for each structure we presented. It can also be seen that the width of the plateau corresponds to an interval of about 0.15 eV or $6kT/q$. These features seem characteristic of the ionization of a localized level in the silicon band gap.

(2) The defect centers are not localized in the interface plane. The observed modifications of the $C_{HF}(V)$ curves can only be explained by a modification in the space charge density in the semiconductor. This shows that the ionized centers must be distributed in the silicon, outside the interface plane.

(3) The defect is a donor and only stands in a small interfacial layer in the silicon.

Although, for an n-type structure in inversion the minimum $C_{HF\infty}$ gives for N_D a value larger than the bulk doping concentration, this is no longer the case with p-type structures (e.g., in fig. 28c, N_A from $C_{HF\infty}$ is 7.25×10^{14} cm^{-3} and the measured bulk doping concentration is $N_A = 7.4 \times 10^{14}$ cm^{-3}). This can be explained if we assume the defect to be a donor center (states of charge +,0) and to be present in a small interfacial layer of the silicon only.

(a) Such a center does not modify the bulk doping concentration.

(b) In an n-type structure, the center is positively ionized when the structure is in inversion and the space charge layer concentration is greater, i.e. $C_{HF\infty}$ is greater.

(c) In a p-type structure in inversion the center is neutral and the observed doping concentration is the same as in the bulk.

Finally, from the apparent interface state density which is introduced by this defect, we can deduce its concentration N_R by means of eq. (2). We found $N_R \simeq 10^{16}$ cm^{-3} for the various structures which we studied. Although this concentration value is very high, it could be explained by the high disorder of the interfacial layer. The observed defect could be introduced during the oxidation process. We are now doing annealing experiments and measurements on $\langle 111 \rangle$ anodically oxidized structures in order to get some information on these points.

6. Conclusion

In order to study the SiO–Si interface, we proposed two measurement methods of the MOS capacitance under conditions of total reversibility.

The knowledge of the low frequency MOS capacitance permits us to determine the apparent interface state density in the *whole* band gap of the silicon and on the *same* structure. From our experimental results we may point out the following conclusions:

(1) A fast increase of the interface state density near the band edges is

systematically observed. The curves $N_{ss}(\psi_s)$ vary in this region almost like the electrostatic field versus surface potential. To interpret this correlation, we suppose that there is in the interfacial layer of the oxide an equal number of positively and negatively charged traps which can move towards or outwards the interface under the action of the very strong surface electrostatic field. This model can give an interpretation of the results given by Jund and Woehrn[4]) and Arnold[3]), who observed the same increase in interface state density near the band edges, and of the results given by Gray and Brown[2]), who did not observe such an increase.

(2) In the structure showing an important apparent interface state density, together with an important flat band translation, the shape of the $N_{ss}(\psi_s)$ curves can be theoretically predicted from the effect of the spatial fluctuations of the surface potential.

Lithium ion migrations in the oxide of MOS structures confirmed the importance of these fluctuations. These experiments showed that the standard deviation was roughly proportional to the mean image charge $\bar{Q}_i$. This result could help to interpret the observed correlation between the apparent interface state density and the fixed oxide charge Q_f.

(3) As it is well known[1]), the MOS capacity grown on silicon slices of surface orientation $\langle 111 \rangle$ show an interface state density larger than in the homologous $\langle 100 \rangle$ structures. But their $C_{LF}(V)$ and $C_{HF}(V)$ and $N_{ss}(\psi_s)$ curves show peculiarities which can be attributed to a defect localized in a small layer of the silicon, near the interface. This defect introduces a deep level at $E_v + 0.35$ eV in the silicon band gap.

In this study, the very low frequency MOS capacitance measurements have been a powerful tool in helping us to show some new characteristic features of the SiO_2–Si interface.

Acknowlegments

We wish to thank Dr. J. Grosvalet for helpful discussions and advice, and Drs. R. Poirier and G. Nuzillat from Sescosem Research Center (Corbeville-Orsay, France) for providing many oxidized slices.

List of symbols

c_n, c_p	Electron and hole capture coefficients on interface states
$C_D(\psi_s)$	Differential space charge capacitance (F cm^{-2})
C_{FB}	MOS capacitance for flat band conditions (F cm^{-2})
$C_{HF}(V)$	Low frequency differential capacitance of MOS structure for a biasing potential V (F cm^{-2})
$C_{HF\,lim}(V)$	Very high frequency limit for $C_{HF}(V)$ (F cm^{-2})

$C_{HF\infty}$	Inversion limit for $C_{HF}(V)$ (F cm^{-2})
C_I	Inversion layer capacitance (F cm^{-2})
$C_{LF}(V)$	Low frequency differential capacitance of MOS structure for a biasing potential V (F cm^{-2})
C_{ox}	Oxide capacitance (F cm^{-2})
C_R	Deep level center capacitance (F cm^{-2})
$C_{ss}(\psi_s)$	Interface state capacitance (F cm^{-2})
$C_{TH}(V)$	Theoretical MOS capacitance (F cm^{-2})
e_{ox}	Oxide thickness (cm)
E_c, E_v	Conduction and valence band limits (eV)
E_F	Fermi level (eV)
E_i	Mid gap energy (eV)
E_R	Defect or impurity level (ev)
f	Frequency
f_{R0}	Fermi function for a defect level
$f(\theta, u)$	Fermi function for an energy level at θ (kT/q units) from mid-gap
G_{nR}	Equivalent conductance between a defect level and conduction band
G_{pR}	Equivalent conductance between a defect level and valence band
G_R	Equivalent conduction of generation recombination phenomena in space charge
$n(x)$	Carrier densities in x-plane (cm^{-3})
$n_0(x)$, $p_0(x)$	Equilibrium carrier densities in x plane established by the dc bias (cm^{-3})
n_{0b}, p_{0b}	Equilibrium bulk carrier densities (cm^{-3})
n_s, p_s	Interface carrier densities (cm^{-3})
N	Number of fixed charges in the oxide of an elementary capacitance
$\bar{N}$	Mean value of N
N_A	Doping acceptor concentration (cm^{-3})
N_D	Doping donor concentration (cm^{-3})
N_R	Density of semiconductor defect introducing a deep level in band gap
$N_{ss}(\theta)$	Density of interface state (cm^{-2} V^{-1}) at a distance θ from mid gap
$N_{ss}(\psi_s)$	Density of interface state occupying the position $\theta = -\psi_s$ in band gap
$N'_{ss}(\psi_s)$	Interface state density determined from $C_{LF}(V)$ and $C_{HF}(V)$
P	Probability
Q	Charge of the MOS capacitance (C)
Q_f	Density of fixed charge in the oxide (C cm^{-2})
$\bar{Q}_f$	Mean value of Q_f
Q_i	Image charge density (C cm^{-2})

$\bar{Q}_i$	Mean value of Q_i
q	Electron charge (C)
t	Time (s)
T	Temperature (°K) or Signal period (s)
$u(x)$	Electrostatic reduced potential (in kT/q units), $u(x)=\beta\psi(x)$
u_b, u_s	Values of u in the bulk and in the interface plane
V	Bias potential (V)
V_{FB}	Value of V for flat band conditions (V)
W	Space charge width (cm)
x	Distance from the interface plane
x_I	Inversion layer width
x_R	Distance, from the interface, of the plane in which Fermi levels go through the deep level θ_R
$\mathscr{A}$	Area of the metallization (cm^2)
$\mathscr{E}_s$	Surface electric field
α	Area of elementary capacitance (cm^2)
β	q/kT
Γ_{ox}	Elementary oxide capacitance ($F\ cm^{-2}$)
Γ_{sp}	Elementary space charge capacitance ($F\ cm^{-2}$)
Γ_{ss}	Elementary interface state capacitance ($F\ cm^{-2}$)
ε_c	Permittivity of free space ($F\ cm^{-1}$)
ε_{si}	Dielectric constant for silicon
θ	Energy interval between a given energy level and mid gap (positive towards valence band, in kT/q units)
θ_R	Value of θ for a defect level
σ_{Q_i}	Standard deviation function of image charge density ($C\ cm^{-2}$)
σ_n, σ_p	Capture cross-sections for electron and hole, respectively (cm^2)
τ_n, τ_p	Relaxation time for charge exchange between interface states and conduction and valence band, respectively
φ_n, φ_p	Pseudo Fermi potential, respectively for electrons and holes
ϕ	Fermi potential (V): $\phi=-E_F/q$
$\psi(x)$	Electrostatic potential in x plane associated to mid gap and measured from Fermi potential
ψ_b	Electrostatic potential value in the bulk
ψ_s	Electrostatic potential value in the plane of the interface, $\psi_s=\psi(x=0)$

References

1) E. H. Nicollian and A. Goetzberger, Bell System Tech. J. **66** (1967) 1055.
2) P. V. Gray and D. M. Brown, Appl. Phys. Letters **8** (1966) 31; see also: D. M. Brown and P. V. Gray, J. Electrochem. Soc. **115** (1968) 760.
3) E. Arnold, IEEE Trans. Electron Devices **ED-15** (1968) 1003.

see also: E. Arnold, in: *Colloque Intern. sur les Propriétés et Utilisations des Structures MIS*, Grenoble, June 1969, Ed. J. Borel (C.N.R.S., Grenoble, France).
4) C. Jund and D. Woehrn, in: *Colloque Intern. sur les Propriétés et Utilisations des Structures MIS*, Grenoble, June 1969, Ed. J. Borel (C.N.R.S., Grenoble, France).
5) W. Fahrner and A. Goetzberger, Appl. Phys. Letters **17** (1970) 16.
6) R. Castagné, Etude de l'Interface SiO_2–Si par Mesures de Capacité en Très Basses Fréquences, PhD Thesis (No. 680 Série A), Orsay, 1970.
7) L. M. Terman, Solid State Electron. **5** (1962) 285.
8) A. Goetzberger, in: *Colloque Intern. sur les Propriétés et Utilisations des Structures MIS*, Grenoble, June 1969, Ed. J. Borel (C.N.R.S., Grenoble, France).
9) E. Arnold, J. Ladell and G. Abowitz, Appl. Phys. Letters 13 (1968) 413.
10) A. Goetzberger, V. Heine and E. H. Nicollian, Appl. Phys. Letters **12** (1968) 95.
11) F. P. Heiman and G. Warfield, IEEE Trans. Electron Devices **ED-12** (1965) 167.
12) H. Preier, Appl. Phys. Letters **10** (1967) 361.
13) C. N. Berglund, IEEE Trans. Electron Devices **ED-13** (1966) 701.
14) R. Castagné, Compt. Rend. (Paris) B **267** (1968) 866.
15) C. T. Sah, R. F. Pierret and A. B. Tole, Solid State Electron. 12 (1969) 681.
16) D. Estève, Thèse de Doctorat d'Etat, Faculté des Sciences de l'Université de Toulouse, 1969, No. 339.
17) R. Castagné and A. Vapaille, Compt. Rend. (Paris) B **270** (1970) 1347.
18) R. Castagné and A. Vapaille, Electron. Letters **6** (1970) 691.
19) R. Castagné and A. Vapaille, Compt. Rend. (Paris) B **270** (1970) 552.
20) M. Kuhn, Meeting of the Electrochem. Soc., New York, May 1969. Recent News Paper Abstract 345, J. Electrochem. Soc. **116** (1969) 249c.
21) M. Kuhn, Solid State Electron. **13** (1970) 873.
22) D. R. Kerr, in: *Colloque Intern. sur les Propiétés et Utilisations des Structures MIS*, Grenoble, June 1969, Ed. J. Borel (C.N.R.S., Grenoble, France).
23) R. Castagné, P. Hesto and A. Vapaille, Compt. Rend. (Paris) B **268** (1969) 1578.
24) E. R. Lindner, Solid State Electron. **13** (1970) 1597.
25) A. Goetzberger, IEEE Trans. Electron Devices **ED-15** (1968) 1009.
26) F. L. Heiman, IEEE Trans. Electron Devices **ED-13** (1966) 855.
27) K. Lehovec, Solid State Electron. **11** (1968) 135.
28) F. Berz, Solied State Electron. **13** (1970) 631.